HHS Public Access

Author manuscript

Cell. Author manuscript; available in PMC 2020 January 10.

Published in final edited form as:

Cell. 2019 January 10; 176(1-2): 334–347.e12. doi:10.1016/j.cell.2018.11.010.

Fibrinogen-like protein 1 is a major immune inhibitory ligand of LAG3

Jun Wang[1], **Miguel F. Sanmamed**[1], **Ila Datar**[2], **Tina Tianjiao Su**[1], **Lan Ji**[1], **Jingwei Sun**[1], **Ling Chen**[3], **Yusheng Chen**[4], **Gefeng Zhu**[1], **Weiwei Yin**[5], **Linghua Zheng**[1], **Ting Zhou**[1], **Ti Badri**[1], **Sheng Yao**[1], **Shu Zhu**[1], **Agedi Boto**[1,2], **Mario Sznol**[6], **Ignacio Melero**[7], **Dario A. A. Vignali**[8,9], **Kurt Schalper**[2], and **Lieping Chen**[1,3,6,10,*]

[1]Department of Immunobiology, Yale University, New Haven, Connecticut, 06511, USA

[2]Department of Pathology, Yale University, New Haven, Connecticut, 06510, USA

[3]Immunotherapy Institute, Fujian Medical University, Fuzhou, Fujian, 350108, China

[4]Provincial Clinical Medical College, Fujian Medical University, Fuzhou, Fujian, 350108, China

[5]Key Laboratory for Biomedical Engineering of Ministry of Education, College of Biomedical Engineering and Instrument Science, Zhejiang University, Hangzhou, 310027, China

[6]Department of Medicine (Medical Oncology), Yale University, New Haven, Connecticut, 06510, USA

[7]Department of Immunology and Immunotherapy, University of Navarra, Pamplona, 31008, Spain

[8]Department of Immunology, University of Pittsburgh, Pittsburgh, Pennsylvania, 15213, USA

[9]Tumor Microenvironment Center, UPMC Hillman Cancer Center, Pittsburgh, Pennsylvania, 15232, USA

[10]Lead Contact

SUMMARY

Lymphocyte-activation gene 3 (LAG3) is an immune inhibitory receptor, with major histocompatibility complex class II (MHC-II) as a canonical ligand. However, it remains controversial whether MHC-II is solely responsible for the inhibitory function of LAG3. Here, we

*Correspondence: lieping.chen@yale.edu.

Author Contributions

Conceptualization, J.W.,M.F.S.,L.C.; Methodology, J.W., M.F.S., I.D., T.T.S., L.J., L.C., J.S., S.Y., G.Z.; Software, J.W., M.F.S., T.T.S., I.D., W.Y.,T.Z., S.Z.; Formal Analysis, J.W., M.F.S., T.T.S., I.D., W.Y., A.B.,L.C.; Investigation, J.W., M.F.S., T.T.S., L.J., I.D., L.C., J.S., T.B.; Resources, L.Z., T.Z., S.Y., M.S., I.M., D.A.A.V., Y.C., K.S., L.C., Writing-Original Draft, J.W., L.C.; Review & Editing, J.W., L.C., T.T.S., M.F.S., D.A.A.V., M.S., I.M., K.S.; Visualization, J.W., M.F.S., L.C.; Supervision, L.C.; Project Administration, J.W., L.C.; Funding Acquisition, L.C.

Declaration of Interests:

LC is a consultant/advisory board member and receives consulting fees from Pfizer, Vcanbio, and GenomiCare; is a scientific founder of NextCure and TAYU Biotech and has sponsored research grants from Boehringer Ingelheim and NextCure. There is a patent application pending related to this work.

demonstrate that fibrinogen-like protein 1 (FGL1), a liver-secreted protein, is a major LAG3 functional ligand independent from MHC-II. FGL1 inhibits antigen-specific T-cell activation and ablation of FGL1 in mice promotes T-cell immunity. Blockade of the FGL1/LAG3 interaction by monoclonal antibodies stimulates tumor immunity and is therapeutic against established mouse tumors in a receptor-ligand inter-dependent manner. FGL1 is highly produced by human cancer cells and elevated FGL1 in the plasma of cancer patients is associated with a poor prognosis and resistance to anti-PD-1/B7-H1 therapy. Our findings reveal an immune evasion mechanism and have implications for the design of cancer immunotherapy.

Graphical Abstract

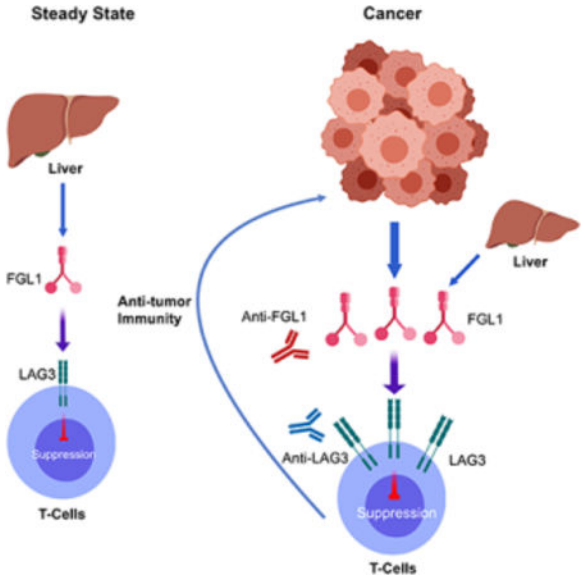

In Brief

FGL1 is identified as a major ligand for the inhibitory receptor LAG3 and its blockade can potentiate anti-tumor T cell responses

Keywords

Cancer; immunology; immunotherapy; tumor immune-evasion mechanism; LAG3; FGL1

INTRODUCTION

Lymphocyte-activation gene 3 (LAG3, CD223) is a transmembrane protein primarily found on activated T cells (Anderson et al., 2016; Andrews et al., 2017; Triebel et al., 1990). LAG3 protein consists of four extracellular immunoglobulin (Ig)-like domains (D1-D4) with high homology to CD4 (Triebel et al., 1990). LAG3 expression can be upregulated by IL-2 and IL-12 on activated T cells (Annunziato et al., 1997; Annunziato et al., 1996; Bruniquel et al., 1998), where it mainly functions as a receptor that delivers inhibitory signals (Huard et al., 1996; Huard et al., 1994; Workman et al., 2002a). LAG3 negatively regulates the proliferation, activation, effector function, and homeostasis of both CD8+ and CD4+ T cells,

as shown in LAG3 knockout mice and antibody studies (Huard et al., 1994; Workman et al., 2004; Workman et al., 2002a; Workman et al., 2002b; Workman and Vignali, 2003, 2005). LAG3 may represent an “exhaustion” marker for CD8+ T cells similar to PD-1 in response to repetitive antigen stimulation in chronic viral infections or cancers (Blackburn et al., 2009; Chihara et al., 2018; Grosso et al., 2009; Grosso et al., 2007; Matsuzaki et al., 2010; Williams et al., 2017). Additionally, LAG3 is also constitutively expressed on a subset of regulatory T-cells and contributes to their suppressive function (Camisaschi et al., 2010; Gagliani et al., 2013; Huang et al., 2004). Currently, monoclonal antibodies (mAbs) that block the interaction of LAG3 with its canonical ligand, MHC-II, are being evaluated for their antitumor activity in clinical trials (Anderson et al., 2016; Ascierto et al., 2017; Rotte et al., 2018).

The major ligand that mediates the immune suppressive functions of LAG3, however, remains controversial. Initial studies by Baixeras and colleagues showed an interaction between MHC-II and LAG3 via a cell-cell adhesion assay (Baixeras et al., 1992), which was further extended by studies indicating LAG3 fusion protein binding to MHC-II+ B cell lines (Huard et al., 1996; Huard et al., 1995). However, there is a lack of direct evidence for the protein-protein interaction between LAG3 and MHCII. MHC-II was proposed to interact with LAG3 through the residues on the membrane-distal, top face of the LAG3 D1 domain (Huard et al., 1997). Functionally, the MHC-II/CD4 interaction supported helper T cell activation, while overexpression of LAG3 downregulated antigen-dependent CD4+ T cell responses *in vitro* (Workman and Vignali, 2003). However, several mAbs that do not block the binding of LAG3 to MHC-II nonetheless promoted T cell functions. For example, C9B7W, a specific mAb against the murine LAG3 D2 domain, enhanced the proliferation and effector functions of T cells *in vitro* and *in vivo* (Workman et al., 2004; Workman et al., 2002b; Workman and Vignali, 2005). This antibody also increased the accumulation and effector function of tumor-specific CD8+ T cells in several tumor models (Grosso et al., 2007; Woo et al., 2012). The effects of C9B7W mAb on T cells are largely similar, if not identical, to those produced by LAG3 genetic deficiency (Woo et al., 2012; Workman and Vignali, 2005). A recent study also showed that anti-LAG3 mAb that do not block MHCII binding could still stimulate T cell activation and anti-tumor activity (Cemerski, 2015). Given that LAG3 also suppresses the function of CD8+ T cells and NK cells, which do not interact with MHC-II (Anderson et al., 2016), these studies raise the possibility that the immunological functions of LAG3 might be mediated via an unknown ligand.

Here we report that fibrinogen-like protein 1 (FGL1) is a major functional ligand of LAG3. FGL1 belongs to the fibrinogen family with high amino acid homology to the carboxyl terminus of the fibrinogen beta- and gamma-subunits, but it does not have the characteristic platelet-binding site, crosslinking region, and thrombin-sensitive site necessary for fibrin clot formation (Yamamoto et al., 1993). Under normal physiological conditions, FGL1 protein is primarily secreted from hepatocytes and contributes to its mitogenic and metabolic functions (Demchev et al., 2013; Hara et al., 2001; Li et al., 2010; Liu and Ukomadu, 2008; Yamamoto et al., 1993; Yan et al., 2002). The immunological function of FGL1, however, remains unknown. Our results demonstrate that FGL1 is a major inhibitory ligand for LAG3, revealing a new mechanism of immune evasion.

RESULTS

FGL1 is an MHC class II-independent high affinity ligand of LAG3

We employed our Genome-Scale Receptor Array (GSRA) technology to search for LAG3 binding protein(s) using an immunoglobulin (Ig) Fc-tagged LAG3 extracellular domain fusion protein (LAG3-Ig) (Figure 1a). The GSRA is a semi-automatic gene expression and detection system for rapidly identifying protein-protein interactions, which has been modified from our previous report (Yao et al., 2011). In this updated system, individual human cDNA encoding transmembrane and secreted proteins (upon addition of a transmembrane domain) were overexpressed on the surface of 293T cells. Several adaptor genes were also expressed in 293T (293T.2A cells) to facilitate protein expression on the cell surface (Figure 1a). An Ig-tagged protein of interest can then be screened for interaction(s) using the GSRA system in a high throughput fashion by the mix-and-read laser scanning macro-confocal fluorescent plate reader. The current version of the GSRA contains over 90% of annotated genes encoding human transmembrane (~5,600) and secreted (~1,000) proteins (Table S1). FGL1 was identified as a major binding protein for LAG3-Ig in the GSRA system (Figure S1a and Figure 1b). The FGL1/LAG3 interaction is conserved across species in both human and mouse (Figure 1b). This interaction was further validated by flow cytometry, as indicated by a linear association between FGL1Ig and anti-LAG3 staining on LAG3+ cells (Figure 1c). The FGL1/LAG3 interaction was shown to have a *Kd* value of ~1.5 nM by Octet bio-layer interferometry analysis (Figure 1d). Using an SEC650 size exclusion column, the purified recombinant FLAG-tagged FGL1 (FLAG-FGL1) showed an oligomeric state (peak1–2) and a dimeric peak (peak 3) (Figure S1b), which was validated via size exclusion chromatography with Multi-Angle Light Scattering analysis (SEC-MALS, data not shown). We observed stronger binding of the oligomeric forms of FLAG-FGL1 (peak 1–2) than the dimeric form (peak 3) to immobilized LAG3-Ig in the Octet analysis (Figure S1c). In addition, the slow disassociation rate hints at a stable interaction between FGL1 and LAG3 in both human and mouse (Figure 1d and Figure S1d). FGL2, a homolog of FGL1 previously implicated in Treg functions (Shevach, 2009), as well as other fibrinogen domain-containing family members such as angiopoietin-related proteins, did not bind LAG3 (Figure 1b and data not shown), indicating that the FGL1/LAG3 interaction is highly specific.

FGL1 is composed of a coil-coil domain (CCD) and a fibrinogen-like domain (FD) (Yamamoto et al., 1993). Through domain deletion studies, we demonstrated that the FD, but not CCD, is responsible for LAG3 binding (Figure S1e). The LAG3 protein consists of four Ig-like extracellular domains, D1-D4 (Huard et al., 1997; Triebel et al., 1990) (Figure 1e, left panel). The deletion of the D3-D4 domain in LAG3 did not affect FGL1 binding, while either D1 or D2 alone partially decreased the binding (Figure 1e, right panel), suggesting that both D1 and D2 contribute to the FGL1/LAG3 interaction. A single point mutation (Y73F) in the C' strand of LAG3 D1 domain was previously shown to disrupt MHC-II binding (Huard et al., 1997; Workman et al., 2002a). However, this mutation did not affect FGL1-Ig binding (Figure 1e, right panel), indicating that the FGL1/LAG3 interaction is nonredundant with MHC-II/LAG3 binding. Furthermore, pre-incubation of LAG3+ 293T cells with C9B7W, an anti-LAG3 mAb that binds the LAG3 D2 domain without blocking

the FGL1/MHC-II interaction (Andrews et al., 2017; Cemerski, 2015; Workman et al., 2002b), led to complete abrogation of FGL1/LAG3 binding (Figure 1f). Finally, LAG3+ cells stained with MHC-II (I-A^b) fusion protein did not show a significant decrease in binding even in the presence of a 100-fold excess of FGL1-Ig (Figure S1f). Taken together, our results indicate that FGL1 interacts with LAG3 in an MHC-II independent manner, and that this interaction involves the FGL1 fibrinogen-like domain and the LAG3 D1-D2 domain.

FGL1 inhibits antigen-mediated T cell responses via LAG3 *in vitro* and *in vivo*

LAG3 is not found on resting T cells other than a subset of Tregs but can be upregulated under various antigen stimulation conditions (Baixeras et al., 1992; Triebel et al., 1990; Workman et al., 2002b). FGL1-Ig fusion protein did not bind resting T cells which express minimal LAG3 levels (data not shown), though it did bind activated T cells from wild type (WT) but not from LAG3-KO mice, as determined via flow cytometry analysis (Figure 2a). Inclusion of FGL1-Ig partially suppressed WT splenic T cell proliferation under suboptimal anti-CD3 stimulation, but this suppression was diminished using LAG3-KO splenocytes (Figure 2b), indicating that the suppressive effect of FGL1-Ig is dependent on LAG3. Similarly, FGL1 better suppressed the antigen-specific induction of IL-2 from a murine LAG3 overexpressing 3A9 T cell line (3A9-LAG3) in a dose dependent fashion compared to the parental 3A9 cell line with low endogenous LAG3 expression (Figure 2c). We generated a mAb specific for mouse FGL1 (clone 177R4) that blocks FGL1-Ig binding to LAG3+ 293T cells in a similar manner to anti-LAG3 mAb C9B7W (Figure S2a–b). Both mAbs abrogated the suppression of FGL1 on IL-2 production from 3A9-LAG3 cells (Figure 2d). Upon CD8+ OT-1 transgenic T cell transfer into syngeneic mice and subsequent immunization with chicken ovalbumin peptide antigen, administration of anti-FGL1 mAb 177R4 significantly promoted antigen-specific OT-1 T cell activation in a manner similar to anti-LAG3 mAb, as determined by increased plasma levels of TNF-α and IFN-γ (Figure S2c–d). Thus, our results support that FGL1 is an inhibitory ligand of LAG3.

Fgl1 deficient mice slowly develop spontaneous autoimmune symptoms

We generated a *Fgl1* gene knockout mouse strain (FGL1-KO) on the C57BL/6 background using an agouti color gene modified mouse embryonic stem cell line (JM8) (Pettitt et al., 2009). In WT mice, *Fgl1* mRNA was detected in the liver but not in other organs or hematopoietic cells (Figure S3a). Soluble FGL1 was also detected in mouse blood (Figure S3b) as previously reported (Liu and Ukomadu, 2008). In contrast, FGL1 was not detected in the plasma or liver of FGL1-KO mice via specific sandwich ELISA and western blot analysis, respectively (Figure S3b–c).

FGL1-KO mice have an overall normal appearance, organ size, and litters, indicating that FGL1 does not globally affect the development and growth of mice. However, up to 40% (8/20) of FGL1-KO mice developed spontaneous dermatitis at the age of 8 months or older, showing lymphocyte infiltration in the dermis (Figure S3d–e). At 14–16 months of age, 5/8 female, but not male mice, had elevated levels of anti-double-stranded DNA autoantibodies in their plasma compared to WT mice (Figure S3f). These findings are consistent with the role of FGL1 as an immune suppressive molecule. To evaluate overall changes in the

immune system of this KO strain, we profiled mouse peripheral blood cells by mass cytometry (CyTOF), a single cell high dimensional analysis tool using 32 metal-conjugated mAbs to determine immune cell lineages as well as functional molecules. A recently described unsupervised clustering method named x-shift was also employed (Samusik et al., 2016). Analysis of the total CD45+ hematopoietic cells revealed 22 distinct cell type/subsets (clusters), with small but significant increases in central memory-like CD8+ T cells subsets (cluster 14–15, CD44+ CD62L+ Ly6C+ $CD127^{med}$ Tbet+ Eomes+) and decreases in two B cell subsets (cluster 2 and 4) (Figure 3a–e). All other clusters were similar in FGL1-KO compared to WT mice (Figure 3a–e). There were no major differences in T cells or myeloid cell subsets in peripheral lymphoid tissues including the spleen or liver (data not shown).

These findings indicate that endogenous FGL1 does not affect mouse development and growth, although it may participate in regulating autoimmunity and immune homeostasis in aged mice.

Fgl1 silencing promotes T cell immunity against tumor growth in mouse models

FGL1-KO and LAG3-KO mice were inoculated subcutaneously *(s.c.)* with syngeneic murine MC38 colon cancer cells. Similar to LAG3-KO mice, FGL1-KO mice showed significantly slower tumor growth in comparison to WT mice (Figure 4a). Whereas all of the WT mice reached an endpoint (average mean tumor diameter of 15 mm) within 60 days, ~50% of FGL1-KO or LAG3-KO mice were tumor free beyond 200 days upon MC38 inoculation (Figure 4b). Similarly, both anti-FGL1 and antiLAG3 mAbs significantly controlled tumor growth of established MC38 murine colon (Figure 4c) and Hepa1–6 murine liver cell lines inoculated *s.c.* in syngeneic C57BL/6 mice (Figure S4a). In contrast, the anti-FGL1 and anti-LAG3 mAb antitumor effect was abrogated in Rag1-KO C57BL/6 mice, which are devoid of T and B cells (Figure 4d). Consistent with these findings, depletion of either CD8+ or CD4+ T cells by specific mAbs completely eliminated the anti-tumor effect of both anti-FGL1 and anti-LAG3 mAb in the MC38 tumor model, indicating that the anti-tumor effect of these mAbs is dependent on both CD8+ and CD4+ T cells (Figure S4b).

To exclude the possibility that additional ligands for LAG3 are functionally redundant to FGL1 and contribute to the anti-tumor effect of the anti-LAG3 mAb, we tested the effect of anti-LAG3 mAb in FGL1-KO mice. While the anti-LAG3 mAb suppressed MC38 tumor growth in WT mice, this antitumor effect was completely eliminated in FGL1-KO mice (Figure 4e). The effect of anti-FGL1 was also dependent on LAG3, as this mAb did not have additive effects on tumor growth in LAG3-KO mice (Figure 4f). Therefore, the anti-tumor effect of anti-FGL1 mAb is dependent on LAG3, whereas the effect of anti-LAG3 relies on FGL1 but not MHC-II or other LAG3 ligands. Altogether, our findings support FGL1 as a major ligand for LAG3 to induce T cell suppressive function and immune evasion.

The deficiency of FGL1 significantly reduced MC38 tumor growth while spleen size and the number of lymphocytes in either tumor-draining or non-tumor-draining lymph nodes remained similar (Figure S4c). Analysis of tumor-infiltrating leukocytes (TIL) in tumors excised on day 17 from FGL1KO and WT mice by mass cytometry revealed a significant increase of CD45+ leukocytes in FGL1-KO tumors (Figure S4d). In 22 clusters across CD45+ cells (Figure 5a–b), we found a significant expansion of CD44+ CD62L- PD-1+

Gata3+ effector memory-like CD4+ TIL (cluster 2 and 3), as well as CD44+ Ly6C+ memory-like CD8+ (DeLong et al., 2018; Pihlgren et al., 1996; Walunas et al., 1995) TIL populations (clusters 8–10) in FGL1-KO tumors (Figure 5b–e). In contrast, Treg (cluster 1), NK (cluster 11) or B cells (cluster 14) did not change significantly (Figure 5b–e). Interestingly, a natural killer T (NKT) population (cluster 12) was highly expanded in the FGL1-KO tumors, in comparison with a significant decrease of F4/80+ CD11b+ MHC-II+ $CD11c^{med}$ tumor-associated macrophages (Clusters 15) (Figure 5c–e). Confirming this data, we also observed a significant increase in the absolute number of leukocytes (CD45+ cells), CD8+, and CD4+ TIL per mg of tumor tissues in mice treated with antiFGL1 or anti-LAG-3 mAbs compared to control treated mice (Figure S4e). Furthermore, there was a significant increase in activation/functional markers, such as CD69, Ly6C, granzyme B (GZB), CD4 and FAS, in CD4+ or CD8+ TIL from anti-FGL1 or anti-LAG3 treated mice (Figure S4f). Our results indicate that silencing the FGL1/LAG3 interaction by either genetic knockout or antibody blockade promotes tumor immunity by stimulating T-cell expansion and activation preferentially in the tumor microenvironment.

FGL1 is upregulated in human cancers

FGL1 mRNA and protein expression is largely limited to the liver and pancreas of human normal tissues according to the BioGPS tissue microarray database and proteome analysis (Kim et al., 2014) (Figure S5a). Meta-analysis of the Oncomine databases revealed the upregulation of *FGL1* mRNA in human solid tumors including lung cancer, prostate cancer, melanoma and colorectal cancer compared to normal tissues, with the highest percentage of upregulation (8/23, or 35%) in lung cancer datasets, while its expression appeared to be downregulated in pancreas, liver, and head and neck cancers (Figure S5b). Furthermore, *FGL1* is one of the most upregulated genes in *The Cancer Genome Atlas* (TCGA) database for lung adenocarcinoma (Figure S5c and Table S2). *FGL1* is also significantly upregulated in prostate or breast cancer but is downregulated in liver cancer within this database (Figure S5c).

We established a multiplex quantitative immunofluorescence (QIF) assay to detect FGL1 protein expression on cells and tissues. In addition, a quantitative sandwich ELISA was also established to detect secreted FGL1 in human plasma (see Methods). A 293T line constitutively expressing FGL1 and human tissue samples were utilized to standardize the assay in FFPE preparations and establish the signal detection threshold (Figure S6a). As expected, levels of FGL1 protein were highest in a cell line transfected to express the *FGL1* gene (Figure S6a) and human liver (data not shown), but low/undetectable in mock-transfected cells (Figure S6a) or samples from human testis and skeletal muscle (data not shown). We then evaluated the localized expression of FGL1 in 275 non-small cell lung carcinomas (NSCLC) presented in tissue microarray format (cohort #1, from Yale University, also see Table S3) by simultaneous staining of FGL1 and pan-cytokeratin using multiplex quantitative immunofluorescence (QIF) staining. In NSCLC, FGL1 protein was found localized in tumor cells (the pan-cytokeratin-positive) with minimal expression in the stromal compartment (the pan-cytokeratinnegative) (Figure 6a) and no expression in paired normal lung tissues (Figure S6b). Tissue FGL1 levels showed a continuous distribution in this cohort and ~15% of specimens from NSCLC patients showed elevated expression

(Figure 6b) which was associated with a significantly decreased 5-year overall survival (Figure 6c). Interestingly, there was no association between FGL1 and B7-H1 (PD-L1) expression levels, but high FGL1 in tumor tissue was significantly associated with high LAG3 levels (Figure S6c). In addition, we also found significantly higher plasma FGL1 levels in NSCLC patients compared to healthy donors in two independent cohorts (also see Table S3): #2 (n=18) from University of Navarra, Pamplona, Spain (Figure 6d) and #3 (n=56) from Fujian Medical University, Fuzhou, China (Figure S6d). Of note, there was no difference in plasma FGL1 levels among NSCLC patients with or without metastasis as well as liver injury (Figure S6e). Furthermore, in cohort #2, we found a positive association of tumor FGL1 QIF scores and plasma FGL1 levels (data not shown). Our findings indicate that FGL1 is upregulated in human cancers, especially in NSCLC.

High plasma FGL1 is associated with poor outcomes in patients with anti-PD therapy

To test if FGL1 acts independently from the B7-H1/PD-1 pathway to suppress tumor immunity, we evaluated the association between the baseline plasma FGL1 levels and the efficacy of the B7H1/PD-1 blockade therapy (anti-PD therapy) in metastatic NSCLC patients. In Cohort #2 (also see Table S3 and S4), we found that higher plasma FGL1 levels were associated with worse overall survival in NSCLC patients treated with anti-PD therapy (hazard ratio (HR)=6.8, 95% confidence interval (CI)=1.1–42 and p-value=0.04) (Figure 6e). Similar results were observed in an independent cohort (Cohort #4, from Yale University, also see Table S3 and S4) of metastatic melanoma patients (n=21) treated with anti-PD-1 mAbs (HR=7.9; 95% CI=2.2–27.4 and p-value <0.001) (Figure 6f). Our results suggest that the FGL1/LAG3 interaction is independent from the B7-H1/PD-1 pathway and could potentially contribute to the resistance of anti-PD therapy in human cancers.

We further tested the role of the anti-FGL1/anti-LAG3 in the presence of the B7-H1/PD-1 pathway blockade using the MC38 tumor model. Mice were inoculated *s.c.* with MC38, and established tumors at day 6 were treated with the mAbs. When applied individually, anti-FGL1, anti-LAG3 or antiB7-H1 mAb slowed tumor growth and minimally prolonged survival (Figure 6g). However, anti-FGL1 or anti-LAG3 mAb in combination with anti-B7-H1 mAb significantly improved survival (Figure 6g) and decreased tumor burden (Figure 6h) compared to single mAb treatment. A significant proportion of mice (>30% of mice) treated with the combination therapy were free of tumor for over 150 days (Figure 6g). Our results suggest that the FGL1/LAG3 pathway is an independent tumor immune evasion mechanism, and that blockade of this interaction may synergize with anti-PD therapy.

DISCUSSION

In this study, we have identified and characterized FGL1 as a major ligand of LAG3 that is responsible for its T cell inhibitory function in a receptor-ligand interdependent manner both *in vitro* and *in vivo*. Genetic ablation or mAbs blocking the FGL1/LAG3 interaction enhanced T cell responses and promoted anti-tumor immunity. With limited expression in the majority of normal tissues, FGL1 is upregulated in several human cancers and is associated with a poor prognosis and therapeutic outcome. Together, our findings support the

FGL1/LAG3 pathway as an immune escape mechanism and a potential target for cancer immunotherapy.

Physiological functions of FGL1 are not well understood. Soluble FGL1 protein can be detected in the blood plasma of healthy donors at the nanogram per milliliter (ml) level, while *FGL1* mRNA can only be detected in liver and pancreas across a large panel of normal tissues (Figure S5a), suggesting that FGL1 may be produced by the liver and/or pancreas and subsequently released into the bloodstream. In addition to the reported function in hepatocyte regeneration and metabolism, our findings reveal for the first time a prominent role of FGL1 in the negative regulation of inflammatory immune responses. FGL1-KO mice spontaneously developed several autoimmune symptoms including dermatitis and antidsDNA autoantibodies (Figure S3d–f). However, these symptoms developed only in the aged but not in newborn or young adult mice, indicating that endogenous FGL1 is not a major regulator for selftolerance but may suppress environmentally induced inflammation. Interestingly, liver is considered an immune-privileged organ, as allogeneic liver transplants can survive longer without immune suppressive agents (Horst et al., 2016). The underlying mechanism for this immune privilege, however, is largely unknown. We did not observe significant liver inflammation in aged FGL1-KO mice (data not shown), perhaps due to a lack of LAG3 expression on resting T cells in the liver. While FGL1 may play a local role in maintaining the tolerogenic environment of the liver, its secretion as a soluble factor allows for potential cross-talk between the liver and other peripheral tissues that may help fine-tune systemic inflammation. This normal physiological function of FGL1 may be hijacked by several solid tumors that increase FGL1 expression to suppress local anti-tumor immunity. In this context, immune evasion may be mediated by high levels of FGL1 in the tumor microenvironment through the interaction with LAG3 specifically expressed on tumor-infiltrating T cells. Our results in mouse tumor models indicate a preferential activation of T cell immunity in the tumor microenvironment upon FGL1/LAG3 blockade while the effect of this blockade in systemic immune suppression is minimal (Wang *et.al*, unpublished observation), suggesting a major role for FGL1 in immune suppression of the tumor microenvironment.

Our results support FGL1 as a major ligand for the T cell inhibitory function of LAG3. First, FGL1/LAG3 represents a high affinity interaction that is specific and physiological, as indicated by fusion protein binding experiments involving primary T cells from WT or *Lag3* deficient mice. Second, FGL1 mAb has similar effects to anti-LAG3 on the stimulation of T cell responses and antitumor effect in our *in vitro* and *in vivo* experiments. Furthermore, anti-FGL1 mAb has no antitumor effect in LAG3 deficient mice while anti-LAG3 mAb likewise loses efficacy in *Fgl1* deficient mice. Finally, our preliminary studies indicate that adult *Fgl1* deficient mice are also prone to the induction of autoimmune diseases (Wang et al, unpublished data), a phenotype similar to LAG3 deficient mice (Bettini et al., 2011; Woo et al., 2012).

To date, at least four different proteins have been reported to interact with LAG3 including MHCII, galectin-3, LSECtin, and α-synuclein. Galectin-3 and LSECtin have potential roles in T cell regulation, while α-synuclein is possibly involved in the neurological function of LAG3 (Kouo et al., 2015; Mao et al., 2016; Xu et al., 2014). The interaction modality of

galectin-3 and LSECtin to LAG3 are less known, but both molecules have previously been shown to have several other binding partners (Kizuka et al., 2015; Li et al., 2009; Liu et al., 2004; Stillman et al., 2006; Tang et al., 2010). It remains to be shown whether their roles in the suppression of T cell-responses and antitumor immunity are dependent on LAG3. Although MHC-II is the first identified ligand for LAG3, the detailed biochemistry and affinity of this interaction is still unclear. Given that FGL1 does not compete with MHC-II for LAG3 binding (Figure S1f), this opens the possibility for the existence of a FGL1/MHC-II/LAG3 trimolecular complex -open questions include the signaling outcome of FGL1 versus MHC-II upon interaction with LAG3 and how this complex could contribute to T cell suppression. A detailed stoichiometry analysis may be required to understand how soluble FGL1 triggers cell surface LAG3 to transmit signals for T cell suppression, which is currently unknown. We found that FGL1 could form oligomers, and these oligomeric forms of FGL1 bound to LAG3 much better than the dimeric form (Figure S1b, c), implicating that oligomeric FGL1 may be required for T cell suppression. The presence of native oligomeric FGL1 may also explain our results in the Octet assay showing a high affinity interaction of purified soluble FGL1 with LAG3. Thus, increased avidity of FGL1, most likely through oligomerization, but potentially through other mechanisms such as attachments to the extracellular matrix, may facilitate its interaction with LAG3 *in vivo*. Currently, several MHC-II blocking anti-LAG3 mAbs are being evaluated in clinical trials for the treatment of advanced human cancer. Preliminary data of these trials showed minimal or modest effect as a single agent (Ascierto and McArthur, 2017; Ascierto et al., 2017). Based on our findings, a possible interpretation for the clinical results could be that these mAbs block the MHC-II/LAG3 interaction but do not block FGL1/LAG3 binding. Thus, these mAbs may still allow FGL1 to transmit inhibitory signals to LAG3, leading to an incomplete blockade of LAG3-mediated immune suppression. Our findings warrant careful re-evaluation of therapeutic strategies that aim to block the immune inhibitory function of LAG3.

Our findings support that the FGL1/LAG3 pathway maybe an important immune evasion mechanism and could contribute to current cancer immunotherapy efforts for several reasons. Our studies indicate that FGL1 is a major ligand for LAG3 to suppress T-cell responses and constitute a new target for immune modulation. Furthermore, upregulation of FGL1 on tumor cells but not in normal tissues (Figure S5) may allow for a highly tumor-selective targeting of antibody therapy. In addition, tumor model studies using FGL1-KO mice demonstrate that FGL1 has a potent immune suppressive effect on anti-tumor immunity that is dependent on LAG3. Moreover, FGL1 may be a potential biomarker to predict the outcome of anti-PD therapy, since high plasma FGL1 levels are associated with a worse response to anti-PD therapy in NSCLC and melanoma patients (Figure 6e, f). Lastly, FGL1 blockade also synergizes with anti-B7-H1 blockade in animal models (Figure 6g, h), suggesting that FGL1 and anti-PD dual-blockade may be an alternative treatment for patients who are resistant to antiPD therapy. In summary, our findings identify a functional interaction of the LAG3 pathway and reveal a possible mechanism that tumors may employ for immune evasion, with important implications for developing next generation cancer immunotherapies.

STAR METHODS

CONTACT FOR REAGENT AND RESOURCE SHARING

Further information and requests for resources and reagents should be directed to and will be fulfilled by the Lead Contact, Dr. Lieping Chen (lieping.chen@yale.edu).

EXPERIMENTAL MODEL AND SUBJECT DETAILS

Mice—Female C57BL/6 (B6) mice, *Rag1*−/− (herein referred to as Rag1-KO) and OT-1 Rag1-KO mice at 6–8 weeks old were purchased from Charles River (Wilmington, MA) and Taconic Biosciences (Rensselaer, NY), respectively. *Fgl1* gene conditional knockout mice were obtained from European Mouse Mutant Archive (EMMA), and homologous targeting of this mouse strain was performed in a genetically engineered B6 ES cell (Agouti JM8A). *Fgl1* whole body knockout mice (*Fgl1*−/−, herein referred to as FGL1-KO) were generated by crossing *Fgl1* gene conditional knockout mice with CMV-*Cre* mice (Jackson Laboratory). The *Lag3* whole body knockout mice (*Lag3*−/−, herein referred to as LAG3-KO) were described previously (Workman and Vignali, 2003). All mouse protocols were in accordance with NIH guidelines and approved by the Animal Care and Use Committee of Yale University School of Medicine.

Plasmids, fusion proteins and antibodies—The human cDNA library constructs coding ~5600 full-length plasma membrane proteins and ~1000 secreted proteins were purchased from Genecopoeia (Rockville, MD), Open Biosystems (Huntsville, AL) or were individually cloned by Chen laboratory at Yale. All of the genes used for the GSRA were cloned into a mammalian expression vector. Human and mouse fusion proteins were generated by tagging the extracellular domain with human Ig Fc or 3xFLAG, expressed in 293T cells, and purified by affinity column, or purchased from R&D systems (Minneapolis, MN). The domain deletion plasmids for FGL1 and LAG3 were produced by PCR or GeneArt synthesis (Thermo Fisher, Waltham, MA). Antibodies used in flow cytometry and *in vitro* studies were purchased from BD Biosciences (San Jose, CA), BioLegend (San Diego, CA), or Thermo Fisher (Waltham, MA). Mouse CD8 or CD4 *in vivo* depletion antibodies were purchased from BioXcell (West Lebanon, NH). The hybridoma (clone C9B7W) producing anti-murine LAG3 mAb was described previously (Workman 2002b). The methods to produce and characterize the panels of rat anti-mouse FGL1 and mouse anti-human FGL1 were described previously by immunization with relevant fusion protein (Chen et al., 1992; Dong et al., 2002). The 177m03/177R4 antibodies were also used for flow cytometry and immunohistochemistry. The 177R8 antibody was used for the detection of FGL1 in the mouse liver by western blot.

Human subjects—All four patient cohorts are summarized in Table S3. Cohort #1 (Yale University) included tumor samples in the form of tissue microarrays (TMAs) from 275 NSCLC patients who were not treated with immunotherapy. Cohort #2 (University of Navarra) included plasma samples collected from 18 NSCLC patients who were treated with anti-PD-1 mAbs. Cohort #3 (Fujian Medical University) included plasma samples from 56 NSCLC patients who were not treated with immunotherapy. Cohort #4 (Yale University) included plasma samples from 21 melanoma patients treated with anti-PD-1 mAbs. The

treatment characteristics of patients in cohort#2 and #4 are summarized in Table S4 and the plasma samples were collected before anti-PD-1 treatment. The study protocols were approved by the Institutional Review Boards from each participating institution and all patients signed written informed consents. Human peripheral bloods were obtained by venipuncture and centrifuged to isolate plasma that were stored at −80°C.

METHOD DETAILS

The genome-scale receptor array (GSRA) system—The GSRA system was modified from our previous report (Yao et al, 2011). Other than ~5,600 genes encoding cell transmembrane proteins, over 1,000 genes encoding secreted proteins were also included in the GSRA system. The gene selection criteria include the expression profiles and homology with known immune-related gene families (bioinformatics analysis using BioGPS, Immgen, HPM, UCSC genome browser and NCBI databases). The selected genes coding secreted proteins were fused with an artificial transmembrane domain (TM) from FIBCD1 (TM insertion into the N-terminal) or B7-H6 (TM insertion into the C-terminal) to ensure membrane expression. In each plate, cDNA library plasmids were diluted individually in OptiMEM (4ug/ml) before transferring into 384-well plates (VWR) with 200ul plasmid solution in each well. Two uls of plasmid solution from each well were further transferred into 1536-well plates (Greiner) by a robotic liquid handling system (PlateMate, ThermoFisher) and stored at −80°C. For the assay, 2 ul OptiMEM containing Lipofectamine 3000 per well was added to the plates with a Multidrop Combi robotic dispenser (Thermo Fisher), followed by the addition of 2,000 293T.2A cells (a 293T subline overexpressing DAP10, DAP12, FcRγ and CD3Z) in 4 ul DMEM medium per well. After incubation at 37°C for 18 hrs, 2 ng of LAG3-Ig (human or mouse) and 3 ng of anti-Fc secondary antibody were added into each well. These plates were read 8 hrs later in the Applied Biosystems 8200 cellular detection system (CDS) and analyzed by the CDS 8200 software. Human Fc Receptors were served as internal positive controls within each plate.

Protein-protein interaction analysis—Recombinant proteins were purified by HiTrap Protein A column (GE Healthcare) or anti-FLAG M2 affinity gel (Sigma). In some experiments, different protein fractions of size exclusion chromatography (SEC) by SEC650 column (BioRad) were collected, and then performed for a size exclusion chromatography with Multi-Angle Light Scattering analysis (SEC-MALS) for absolute molecular mass and size measurements using Agilent 1200 system (Agilent Technologies) equipped with Superdex 200 column (GE Healthcare). Protein interactions were measured and analyzed by an Octet Red instrument (PALL, NY). The Octet Protein A sensor was dipped into solution containing mouse or human LAG3-Ig fusion protein (10ug/ml) and subsequently loaded with various concentrations of FLAG tagged FGL1 proteins (two-fold serial dilutions) or their different SEC peak fractions (10ug/ml). Protein association and disassociation was monitored and analyzed by Octet software, and the *Kd* value was calculated using 1:1 binding ratio.

T cell function assays—T cell costimulation assay was described previously (Chapoval et al., 2001; Sica et al., 2003). Briefly, anti-mouse CD3 mAb (eBiosciences) at suboptimal concentrations were pre-coated in 96-well flat plates. Splenocytes from wild-type B6 mice

or LAG3-KO mice at 3×10^5/well were added in the presence of FGL1-Ig or control Ig at 5ug/ml and cultured at 37°C for 3 days. In the last 16 hrs of culture, ^{3}H-TdR was added and counted with a MicroBeta Trilux liquid scintillation counter (PerkinElmer, Waltham, MA). For antigen-specific stimulation, 3A9 T cell hybridoma (with low endogenous LAG3 expression) or 3A9 over-expressing mouse LAG3 gene (3A9-LAG3) was incubated with LK35.2 cell line as antigen-presenting cells in the presence of HEL peptide (1.5ug/ml) and recombinant FGL1 or control protein at the indicated concentrations. Anti-FGL1(177R4) or anti-LAG3 antibodies (5ug/ml) were also included at the beginning of the culture. The IL-2 levels in the supernatant 24 hrs after exposure to antigens were analyzed by CBA kit (BD Pharmingen).

Syngeneic mouse tumor models—Female 8–10-week-old LAG3-KO, FGL1-KO mice or wild-type littermates (WT) were inoculated *s.c.* with MC38 (5×10^5/mouse) or Hepa1–6 (1×10^6/mouse) at day 0 and subsequently treated intraperitoneally (*i.p.*) with 100 ug of anti-FGL1(177R4) or anti-LAG3 (C9B7W) mAbs on days 6, 10, 14 and 18, with saline or rat-Ig as controls. Anti-B7-H1 (10B5) (Dong et al., 2002; Hirano et al., 2005) at 100ug was injected *i.p.* at day 6. Tumor growth was monitored by electronic caliper twice a week and shown as the mean tumor diameter: (length + width)/2(Chen et al., 1992; Chen et al., 1994).

Mouse tissue digestion—Mouse tumor tissues were mechanically dissociated with the GentleMACS Dissociator (Miltenyi Biotec) in the presence of RPMI 1640 with 1mg/ml Collagenase IV plus 0.1mg/ml DNase I (Sigma-Aldrich) for 30 min at 37°C. Cell suspension was washed with RPMI containing 10% FBS (GIBCO) and filtered through 70-μm cell strainer (BD Falcon).

Mass cytometry sample preparation—Cells from tumor tissue were re-suspended in PBS with 0.5% BSA and 0.02% NaN3 and incubated with mAb against mouse CD16/32 for 10 min at room temperature to block Fc receptors. Subsequently metal-labeled mAbs cocktail against cell surface molecules were added and further incubated for 20 minutes on ice. Antibodies were either purchased pre-conjugated from Fluidigm or conjugated in-house using mass cytometry antibody conjugation kits (Fluidigm) according to the manufacturer's instructions. Cells were stained for viability with 5mM cisplatin in FBS (Fluidigm) for 1 minutes on ice. After the treatment with the Fixation/Permeabilization Buffer (Thermo Fisher), cells were further incubated with the metal-labeled mAbs cocktail against intracellular proteins. Cells were then washed and stained with 1 ml of 1:4000 191/193Ir DNA intercalator (Fluidigm) diluted in PBS containing 1.6% Paraformaldehyde (EMS), and stored at 4°C until acquisition.

Mass cytometry sample acquisition—At the moment of acquisition, cells were washed once with PBS with 0.5% BSA and 0.02% NaN3, once with ddH2O, and then re-suspended in ddH2O containing bead standards (Fluidigm) to approximately 10^6 cells per ml. Samples were subsequently acquired on a CyTOF2 machine (Fluidigm) at an event rate of <400 events/second.

Quantitative multiplex immunofluorescence (QIF)—Simultaneous and quantitative multiplex immunofluorescence protocol was developed as previously described (Schalper et

al., 2015) using specific antibodies for indicated antigens carefully titrated and validated individually. Briefly, fresh histology sections from the cases were deparaffinized and subjected to antigen retrieval using EDTA buffer (pH=8.0) and boiled for 20 min at 97°C in a pressure-boiling container (PT module, Lab Vision). Slides were then incubated with dual endogenous peroxidase block (DAKO #S2003, Carpinteria, CA) for 10 min at room temperature and subsequently with a blocking solution containing 0.3% bovine serum albumin in 0.05% Tween solution for 30 minutes. Slides were stained with 4', 6-Diamidino-2-Phenylindole (DAPI) for visualization of all cell nuclei, and simultaneously stained with anti-FGL1 (clone 177m03) as well as antibody to pan-cytokeratin (CK, clone AE1/AE3, Abcam). In some experiments, the slides were co-stained with antibodies to LAG-3 (clone 17B4, Abcam) or B7-H1(clone 405–9A11, Cell signaling). Secondary antibodies and fluorescent reagents were later included for the detection of the signal of each marker, including anti-mouse Envision (K4001, DAKO) with Cy5-tyramide (Perkin-Elmer), anti-mouse IgG1 antibody (Abcam) with Cy3 plus (Perkin-Elmer), goat anti-rabbit (Abcam) with biotinylated tyramide/Streptavidine-Alexa750 conjugate (Perkin-Elmer). Residual horseradish peroxidase activity between incubations with secondary antibodies was eliminated by exposing the slides twice for 10 minutes to a solution containing benzoic hydrazide and hydrogen peroxide.

Measurement of plasma FGL1 levels—Two pairs of anti-FGL1 antibodies were used to measure FGL1 levels in the plasma of human (177m01&177m03) or mouse (177R1&177R4) samples by the sandwiched enzyme-linked immunosorbent assay (ELISA). The assay diluent (PBS with 10%FBS) served as negative control.

QUANTIFICATION AND STATISTICAL ANALYSIS

Mass cytometry data analysis—All mass cytometry files were normalized and manually gated in FlowJo (version X 10.0.7r2) or Cytobank (Santa Clara, CA) by DNA, event length, live/dead discrimination, CD45, and 4 bead channels to exclude dead, debris, doublets, and non-immune cells and beads. Data were arcsinh transformed with a cofactor of 5 before applying the downstream analyses. X-shift clustering analysis (Samusik et al., 2016) in Java was performed to pooled samples to automatically identify underlying immune subsets. Heat-maps were generated with selected markers, which had been normalized by dividing the 99% percentile of cluster mean value for each marker. Cell frequency in each cluster was calculated as the assigned cell events dividing the total cell events in the same sample after manual gating. Clusters with less than 1% cell frequency for all samples were not displayed in frequency plot or heat-maps in order to increase the clarity of visualization. t-Distributed Stochastic Neighbor Embedding (t-SNE) dimension reduction was performed using R package (van der Maaten and Hinton, 2008) to WT/FGL1-KO tumors and PBMC datasets. Each sample was randomly sampled for up to 5,000 cells to ensure the total displayed cell events in WT and FGL1-KO scenarios were equivalent. For analysis of antibody treatment data, FCS files were manually pre-gated on Ir193 DNA $^{+}$CD45^{+} events, excluding cisplatin^{+} dead cells, doublets and DNA-negative debris, and analyzed by Cytobank (Santa Clara, CA).

Tissue fluorescence measurement and scoring—Quantitative measurement of the fluorescent signal was performed using the AQUA® method that enables objective and sensitive measurement of targets within user-defined tissue compartments. Briefly, the QIF score of each marker expression was calculated by dividing the corresponding antibody staining pixel intensities by the area of cytokeratin (CK) positive tumor compartment or the DAPI positive total tissue compartment. Scores were normalized to the exposure time and bit depth at which the images were captured, allowing scores collected at different exposure times to be comparable.

Bioinformatics and statistics—The FGL1 expression pattern in normal human or mouse tissues as well as leukocytes were analyzed in BioGPS and HPM databases. The mRNA microarray data on solid cancers and the counterpart normal tissues (254 datasets in total covering 14 types of human cancers) were collected from Oncomine (Thermo Fisher). *FGL1* upregulation or downregulation frequency in the datasets of each cancer (fold change ≥ 3 for upregulation, or <0.3 for downregulation, and p-value < 0.05 as cutoff) were further analyzed by the program R. Moreover, *FGL1* expression in individual cancer versus counterpart normal tissues was also evaluated using TCGA cancer databases. The original microarray data was normalized by cancer browser (https://genome-cancer.ucsc.edu/) and then analyzed by the program R. Student's ttest, two-way ANOVA, and Log-rank test on GraphPad Prism 7.0 was used for statistical analysis, and p-values reflect comparison to the control samples. P-values were reported as follows: NS, not significant, *, p<0.05; **, p<0.01; ***, p<0.001, ****, p<0.0001. The error bars in figures represent standard error of the mean (SEM).

DATA AND SOFTWARE AVAILABILITY

The CyTOF FCS files associated with the datasets in this paper have been uploaded in Mendeley database with the following preview link: https://data.mendeley.com/datasets/8gvfpy83jn/draft?a=e1bb6f8d-a1f8-481f-a465-142dabd0f24b

Supplemental Excel Table: Supplemental Table S1. Gene list in the GSRA system, related to Figure 1.

Supplemental Excel Table: Supplemental Table S2. The list of top 200 upregulated genes in the TCGA database. Lung adenocarcinoma versus counterpart normal tissues are presented, related to Figure 6.

Supplementary Material

Refer to Web version on PubMed Central for supplementary material.

Acknowledgements

We thank Beth Cadugan for editing the manuscript; Jun Zhao for data analysis, and other members in the laboratories of Yale for helpful discussions and technical assistance, as well as Drs. Tim Zheng, Anne Vogt, Birgit Fogal, Timothy Fenn, Sven Mostboeck, Karl-Heinz Heider, David Blair from Boehringer Ingelheim for their helpful discussion. This research was supported partially by National Institutes of Health grants P30 CA16359, P50 CA196530, a sponsored research funding from Boehringer Ingelheim and an endowment from United Technologies Corporation to L.C. M.F.S. is supported by a Miguel Servet contract from Instituto de Salud Carlos III, Fondo de

Investigación Sanitaria (Spain). D.A.A.V. is supported by National Institutes of Health (P01 AI108545) and NCI Comprehensive Cancer Center Support CORE grant (CA047904).

References

Anderson AC, Joller N, and Kuchroo VK (2016). Lag-3, Tim-3, and TIGIT: Co-inhibitory Receptors with Specialized Functions in Immune Regulation. Immunity 44, 989–1004. [PubMed: 27192565]

Andrews LP, Marciscano AE, Drake CG, and Vignali DA (2017). LAG3 (CD223) as a cancer immunotherapy target. Immunol Rev 276, 80–96. [PubMed: 28258692]

Annunziato F, Manetti R, Cosmi L, Galli G, Heusser CH, Romagnani S, and Maggi E (1997). Opposite role for interleukin-4 and interferon-gamma on CD30 and lymphocyte activation gene-3 (LAG-3) expression by activated naive T cells. Eur J Immunol 27, 2239–2244. [PubMed: 9341765]

Annunziato F, Manetti R, Tomasevic I, Guidizi MG, Biagiotti R, Gianno V, Germano P, Mavilia C, Maggi E, and Romagnani S (1996). Expression and release of LAG-3-encoded protein by human CD4+ T cells are associated with IFN-gamma production. FASEB J 10, 769–776. [PubMed: 8635694]

Ascierto PA, and McArthur GA (2017). Checkpoint inhibitors in melanoma and early phase development in solid tumors: what's the future? J Transl Med 15, 173. [PubMed: 28789707]

Ascierto PA, Melero I, Bhatia S, Bono P, Sanborn RE, Lipson EJ, Callahan MK, Gajewski T, Gomez-Roca CA, Hodi FS, et al. (2017). Initial efficacy of anti-lymphocyte activation gene-3 (anti–LAG-3; BMS-986016) in combination with nivolumab (nivo) in pts with melanoma (MEL) previously treated with anti–PD-1/PD-L1 therapy. Journal of Clinical Oncology 35, 9520–9520.

Baixeras E, Huard B, Miossec C, Jitsukawa S, Martin M, Hercend T, Auffray C, Triebel F, and Piatier-Tonneau D (1992). Characterization of the lymphocyte activation gene 3-encoded protein. A new ligand for human leukocyte antigen class II antigens. J Exp Med 176, 327–337. [PubMed: 1380059]

Bettini M, Szymczak-Workman AL, Forbes K, Castellaw AH, Selby M, Pan X, Drake CG, Korman AJ, and Vignali DA (2011). Cutting edge: accelerated autoimmune diabetes in the absence of LAG-3. J Immunol 187, 3493–3498. [PubMed: 21873518]

Blackburn SD, Shin H, Haining WN, Zou T, Workman CJ, Polley A, Betts MR, Freeman GJ, Vignali DA, and Wherry EJ (2009). Coregulation of CD8+ T cell exhaustion by multiple inhibitory receptors during chronic viral infection. Nat Immunol 10, 29–37. [PubMed: 19043418]

Bruniquel D, Borie N, Hannier S, and Triebel F (1998). Regulation of expression of the human lymphocyte activation gene-3 (LAG-3) molecule, a ligand for MHC class II. Immunogenetics 48, 116–124. [PubMed: 9634475]

Camisaschi C, Casati C, Rini F, Perego M, De Filippo A, Triebel F, Parmiani G, Belli F, Rivoltini L, and Castelli C (2010). LAG-3 expression defines a subset of CD4(+)CD25(high)Foxp3(+) regulatory T cells that are expanded at tumor sites. J Immunol 184, 6545–6551. [PubMed: 20421648]

Cemerski S, Zhao S, Chenard M, Laskey J, Cui L, Shukla R, … De Waal Malefyt R (2015). T cell activation and anti-tumor efficacy of anti-LAG-3 antibodies is independent of LAG-3 – MHCII blocking capacity. Journal for Immunotherapy of Cancer 3(Suppl 2), 183.

Chapoval AI, Ni J, Lau JS, Wilcox RA, Flies DB, Liu D, Dong H, Sica GL, Zhu G, Tamada K, et al. (2001). B7-H3: a costimulatory molecule for T cell activation and IFN-gamma production. Nat Immunol 2, 269–274. [PubMed: 11224528]

Chen L, Ashe S, Brady WA, Hellstrom I, Hellstrom KE, Ledbetter JA, McGowan P, and Linsley PS (1992). Costimulation of antitumor immunity by the B7 counterreceptor for the T lymphocyte molecules CD28 and CTLA-4. Cell 71, 1093–1102. [PubMed: 1335364]

Chen L, McGowan P, Ashe S, Johnston J, Li Y, Hellstrom I, and Hellstrom KE (1994). Tumor immunogenicity determines the effect of B7 costimulation on T cell-mediated tumor immunity. J Exp Med 179, 523–532. [PubMed: 7507508]

Chihara N, Madi A, Kondo T, Zhang H, Acharya N, Singer M, Nyman J, Marjanovic ND, Kowalczyk MS, Wang C, et al. (2018). Induction and transcriptional regulation of the co-inhibitory gene module in T cells. Nature 558, 454–459. [PubMed: 29899446]

DeLong JH, Hall AO, Konradt C, Coppock GM, Park J, Harms Pritchard G, and Hunter CA (2018). Cytokine- and TCR-Mediated Regulation of T Cell Expression of Ly6C and Sca-1. J Immunol 200, 1761–1770. [PubMed: 29358280]

Demchev V, Malana G, Vangala D, Stoll J, Desai A, Kang HW, Li Y, Nayeb-Hashemi H, Niepel M, Cohen DE, et al. (2013). Targeted deletion of fibrinogen like protein 1 reveals a novel role in energy substrate utilization. PLoS One 8, e58084. [PubMed: 23483972]

Dong H, Strome SE, Salomao DR, Tamura H, Hirano F, Flies DB, Roche PC, Lu J, Zhu G, Tamada K, et al. (2002). Tumor-associated B7-H1 promotes T-cell apoptosis: a potential mechanism of immune evasion. Nat Med 8, 793–800. [PubMed: 12091876]

Gagliani N, Magnani CF, Huber S, Gianolini ME, Pala M, Licona-Limon P, Guo B, Herbert DR, Bulfone A, Trentini F, et al. (2013). Coexpression of CD49b and LAG-3 identifies human and mouse T regulatory type 1 cells. Nat Med 19, 739–746. [PubMed: 23624599]

Grosso JF, Goldberg MV, Getnet D, Bruno TC, Yen HR, Pyle KJ, Hipkiss E, Vignali DA, Pardoll DM, and Drake CG (2009). Functionally distinct LAG-3 and PD-1 subsets on activated and chronically stimulated CD8 T cells. J Immunol 182, 6659–6669. [PubMed: 19454660]

Grosso JF, Kelleher CC, Harris TJ, Maris CH, Hipkiss EL, De Marzo A, Anders R, Netto G, Getnet D, Bruno TC, et al. (2007). LAG-3 regulates CD8+ T cell accumulation and effector function in murine self- and tumor-tolerance systems. J Clin Invest 117, 3383–3392. [PubMed: 17932562]

Hara H, Yoshimura H, Uchida S, Toyoda Y, Aoki M, Sakai Y, Morimoto S, and Shiokawa K (2001). Molecular cloning and functional expression analysis of a cDNA for human hepassocin, a liverspecific protein with hepatocyte mitogenic activity. Biochim Biophys Acta 1520, 45–53. [PubMed: 11470158]

Hirano F, Kaneko K, Tamura H, Dong H, Wang S, Ichikawa M, Rietz C, Flies DB, Lau JS, Zhu G, et al. (2005). Blockade of B7-H1 and PD-1 by monoclonal antibodies potentiates cancer therapeutic immunity. Cancer Res 65, 1089–1096. [PubMed: 15705911]

Horst AK, Neumann K, Diehl L, and Tiegs G (2016). Modulation of liver tolerance by conventional and nonconventional antigen-presenting cells and regulatory immune cells. Cell Mol Immunol 13, 277–292. [PubMed: 27041638]

Huang CT, Workman CJ, Flies D, Pan X, Marson AL, Zhou G, Hipkiss EL, Ravi S, Kowalski J, Levitsky HI, et al. (2004). Role of LAG-3 in regulatory T cells. Immunity 21, 503–513. [PubMed: 15485628]

Huard B, Mastrangeli R, Prigent P, Bruniquel D, Donini S, El-Tayar N, Maigret B, Dreano M, and Triebel F (1997). Characterization of the major histocompatibility complex class II binding site on LAG-3 protein. Proc Natl Acad Sci U S A 94, 5744–5749. [PubMed: 9159144]

Huard B, Prigent P, Pages F, Bruniquel D, and Triebel F (1996). T cell major histocompatibility complex class II molecules down-regulate CD4+ T cell clone responses following LAG-3 binding. Eur J Immunol 26, 1180–1186. [PubMed: 8647185]

Huard B, Prigent P, Tournier M, Bruniquel D, and Triebel F (1995). CD4/major histocompatibility complex class II interaction analyzed with CD4- and lymphocyte activation gene-3 (LAG-3)-Ig fusion proteins. Eur J Immunol 25, 2718–2721. [PubMed: 7589152]

Huard B, Tournier M, Hercend T, Triebel F, and Faure F (1994). Lymphocyte-activation gene 3/major histocompatibility complex class II interaction modulates the antigenic response of CD4+ T lymphocytes. Eur J Immunol 24, 3216–3221. [PubMed: 7805750]

Kim MS, Pinto SM, Getnet D, Nirujogi RS, Manda SS, Chaerkady R, Madugundu AK, Kelkar DS, Isserlin R, Jain S, et al. (2014). A draft map of the human proteome. Nature 509, 575–581. [PubMed: 24870542]

Kizuka Y, Kitazume S, Sato K, and Taniguchi N (2015). Clec4g (LSECtin) interacts with BACE1 and suppresses Abeta generation. FEBS Lett 589, 1418–1422. [PubMed: 25957769]

Kouo T, Huang L, Pucsek AB, Cao M, Solt S, Armstrong T, and Jaffee E (2015). Galectin-3 Shapes Antitumor Immune Responses by Suppressing CD8+ T Cells via LAG-3 and Inhibiting Expansion of Plasmacytoid Dendritic Cells. Cancer Immunol Res 3, 412–423. [PubMed: 25691328]

Li CY, Cao CZ, Xu WX, Cao MM, Yang F, Dong L, Yu M, Zhan YQ, Gao YB, Li W, et al. (2010). Recombinant human hepassocin stimulates proliferation of hepatocytes in vivo and improves survival in rats with fulminant hepatic failure. Gut 59, 817–826. [PubMed: 19880967]

Li Y, Hao B, Kuai X, Xing G, Yang J, Chen J, Tang L, Zhang L, and He F (2009). C-type lectin LSECtin interacts with DC-SIGNR and is involved in hepatitis C virus binding. Mol Cell Biochem 327, 183–190. [PubMed: 19234677]

Liu W, Tang L, Zhang G, Wei H, Cui Y, Guo L, Gou Z, Chen X, Jiang D, Zhu Y, et al. (2004). Characterization of a novel C-type lectin-like gene, LSECtin: demonstration of carbohydrate binding and expression in sinusoidal endothelial cells of liver and lymph node. J Biol Chem 279, 18748–18758. [PubMed: 14711836]

Liu Z, and Ukomadu C (2008). Fibrinogen-like protein 1, a hepatocyte derived protein is an acute phase reactant. Biochem Biophys Res Commun 365, 729–734. [PubMed: 18039467]

Mao X, Ou MT, Karuppagounder SS, Kam TI, Yin X, Xiong Y, Ge P, Umanah GE, Brahmachari S, Shin JH, et al. (2016). Pathological alpha-synuclein transmission initiated by binding lymphocyte-activation gene 3. Science 353.

Matsuzaki J, Gnjatic S, Mhawech-Fauceglia P, Beck A, Miller A, Tsuji T, Eppolito C, Qian F, Lele S, Shrikant P, et al. (2010). Tumor-infiltrating NY-ESO-1-specific CD8+ T cells are negatively regulated by LAG-3 and PD-1 in human ovarian cancer. Proc Natl Acad Sci U S A 107, 7875–7880. [PubMed: 20385810]

Pettitt SJ, Liang Q, Rairdan XY, Moran JL, Prosser HM, Beier DR, Lloyd KC, Bradley A, and Skarnes WC (2009). Agouti C57BL/6N embryonic stem cells for mouse genetic resources. Nat Methods 6, 493–495. [PubMed: 19525957]

Pihlgren M, Dubois PM, Tomkowiak M, Sjogren T, and Marvel J (1996). Resting memory CD8+ T cells are hyperreactive to antigenic challenge in vitro. J Exp Med 184, 2141–2151. [PubMed: 8976170]

Rotte A, Jin JY, and Lemaire V (2018). Mechanistic overview of immune checkpoints to support the rational design of their combinations in cancer immunotherapy. Ann Oncol 29, 71–83. [PubMed: 29069302]

Samusik N, Good Z, Spitzer MH, Davis KL, and Nolan GP (2016). Automated mapping of phenotype space with single-cell data. Nat Methods 13, 493–496. [PubMed: 27183440]

Schalper KA, Brown J, Carvajal-Hausdorf D, McLaughlin J, Velcheti V, Syrigos KN, Herbst RS, and Rimm DL (2015). Objective measurement and clinical significance of TILs in non-small cell lung cancer. J Natl Cancer Inst 107.

Shevach EM (2009). Mechanisms of foxp3+ T regulatory cell-mediated suppression. Immunity 30, 636–645. [PubMed: 19464986]

Sica GL, Choi IH, Zhu G, Tamada K, Wang SD, Tamura H, Chapoval AI, Flies DB, Bajorath J, and Chen L (2003). B7-H4, a molecule of the B7 family, negatively regulates T cell immunity. Immunity 18, 849–861. [PubMed: 12818165]

Stillman BN, Hsu DK, Pang M, Brewer CF, Johnson P, Liu FT, and Baum LG (2006). Galectin-3 and galectin-1 bind distinct cell surface glycoprotein receptors to induce T cell death. J Immunol 176, 778–789. [PubMed: 16393961]

Tang L, Yang J, Tang X, Ying W, Qian X, and He F (2010). The DC-SIGN family member LSECtin is a novel ligand of CD44 on activated T cells. Eur J Immunol 40, 1185–1191. [PubMed: 20127679]

Triebel F, Jitsukawa S, Baixeras E, Roman-Roman S, Genevee C, Viegas-Pequignot E, and Hercend T (1990). LAG-3, a novel lymphocyte activation gene closely related to CD4. J Exp Med 171, 1393–1405. [PubMed: 1692078]

van der Maaten L, and Hinton G (2008). Visualizing Data using t-SNE. J Mach Learn Res 9, 2579–2605.

Walunas TL, Bruce DS, Dustin L, Loh DY, and Bluestone JA (1995). Ly-6C is a marker of memory CD8+ T cells. J Immunol 155, 1873–1883. [PubMed: 7543536]

Williams JB, Horton BL, Zheng Y, Duan Y, Powell JD, and Gajewski TF (2017). The EGR2 targets LAG-3 and 4–1BB describe and regulate dysfunctional antigen-specific CD8+ T cells in the tumor microenvironment. J Exp Med 214, 381–400. [PubMed: 28115575]

Woo SR, Turnis ME, Goldberg MV, Bankoti J, Selby M, Nirschl CJ, Bettini ML, Gravano DM, Vogel P, Liu CL, et al. (2012). Immune inhibitory molecules LAG-3 and PD-1 synergistically regulate T-cell function to promote tumoral immune escape. Cancer Res 72, 917–927. [PubMed: 22186141]

Workman CJ, Cauley LS, Kim IJ, Blackman MA, Woodland DL, and Vignali DA (2004). Lymphocyte activation gene-3 (CD223) regulates the size of the expanding T cell population following antigen activation in vivo. J Immunol 172, 5450–5455. [PubMed: 15100286]

Workman CJ, Dugger KJ, and Vignali DA (2002a). Cutting edge: molecular analysis of the negative regulatory function of lymphocyte activation gene-3. J Immunol 169, 5392–5395. [PubMed: 12421911]

Workman CJ, Rice DS, Dugger KJ, Kurschner C, and Vignali DA (2002b). Phenotypic analysis of the murine CD4-related glycoprotein, CD223 (LAG-3). Eur J Immunol 32, 2255–2263. [PubMed: 12209638]

Workman CJ, and Vignali DA (2003). The CD4-related molecule, LAG-3 (CD223), regulates the expansion of activated T cells. Eur J Immunol 33, 970–979. [PubMed: 12672063]

Workman CJ, and Vignali DA (2005). Negative regulation of T cell homeostasis by lymphocyte activation gene-3 (CD223). J Immunol 174, 688–695. [PubMed: 15634887]

Xu F, Liu J, Liu D, Liu B, Wang M, Hu Z, Du X, Tang L, and He F (2014). LSECtin expressed on melanoma cells promotes tumor progression by inhibiting antitumor T-cell responses. Cancer Res 74, 3418–3428. [PubMed: 24769443]

Yamamoto T, Gotoh M, Sasaki H, Terada M, Kitajima M, and Hirohashi S (1993). Molecular cloning and initial characterization of a novel fibrinogen-related gene, HFREP-1. Biochem Biophys Res Commun 193, 681–687. [PubMed: 8390249]

Yan J, Ying H, Gu F, He J, Li YL, Liu HM, and Xu YH (2002). Cloning and characterization of a mouse liver-specific gene mfrep-1, up-regulated in liver regeneration. Cell Res 12, 353–361. [PubMed: 12528893]

Yao S, Zhu Y, Zhu G, Augustine M, Zheng L, Goode DJ, Broadwater M, Ruff W, Flies S, Xu H, et al. (2011). B7-h2 is a costimulatory ligand for CD28 in human. Immunity 34, 729–740. [PubMed: 21530327]

Highlights

- FGL1 is a major ligand of LAG3 that mediates T-cell suppression
- FGL1 is normally released by the liver in low levels but by cancer in high levels
- Blockade of the FGL1/LAG3 interaction potentiates anti-tumor immunity

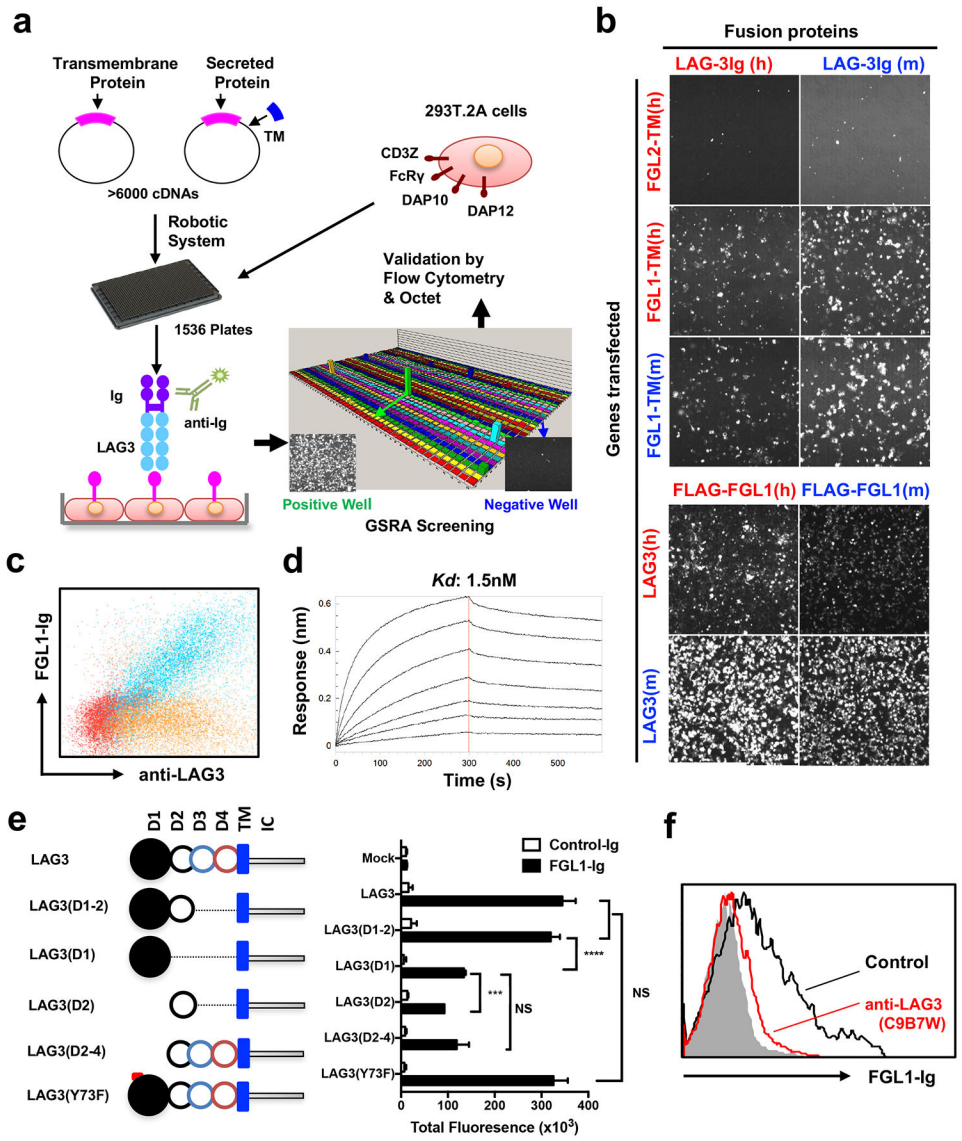

Figure 1. Identification of FGL1 as a binding partner of LAG3 in the GSRA system

(a) Schematic representation of the GSRA system. Individual plasmids of genes encoding both transmembrane and secreted proteins were transfected into 293T.2A cells (see methods and Table S1) in 1,536-well plates. LAG3-Ig as well as fluorescence labeled anti-Fc mAb were added into each well for rapid detection of LAG3-Ig binding. Human Fc receptors served as internal positive controls within each plate. Positive hits were confirmed by flow cytometry or Octet bio-layer interferometry. TM, transmembrane domain.

(b) Image of the FGL1/LAG3 interaction in GSRA system. 293T.2A cells were transfected with human (h) or mouse (m) FGL1-TM or full-length LAG3 as indicated on the Y-axis. Human FGL2-TM was included as a negative control. The indicated fusion proteins shown on the X-axis were added to the culture to evaluate binding to the transfectants by the cellular detection system (CDS).

(c) Representative flow cytometry dot plot of FGL1-Ig binding to mouse LAG3+ 293T.2A (blue) or mock cells (red). Control Ig binding to mouse LAG3+ 293T.2A is also shown (brown).

(d) Representative Octet sensorgrams showing various amounts of FLAG-tagged mouse FGL1 (starting from 10ug/ml, two-fold serial dilutions) binding to immobilized mouse LAG3-Ig.

(e) Schematic representation of constructs coding full-length mouse LAG3, LAG3 Y73F mutant, or LAG3 with different extracellular domain deletions (left). LAG3 full-length protein consists of four extracellular Ig domains (D1 to D4), the transmembrane domain (TM), and intracellular domain (IC) (left). Quantification of FGL1-Ig binding to 293T.2A cells transfected to express LAG3 with domain deletion/mutation (right). Data were analyzed by CDS software and presented as the mean ± SEM. *** $p<0.001$, **** $p<0.0001$, NS, not significant by Student's t-test.

(f) FGL1-Ig binding to mouse LAG3+ 293T.2A cells in the presence of control mAb (black line) or antiLAG3 (red line) by flow cytometry. Cells stained with control Ig (shadow) served as a negative control. All data are representative of at least two independent experiments.

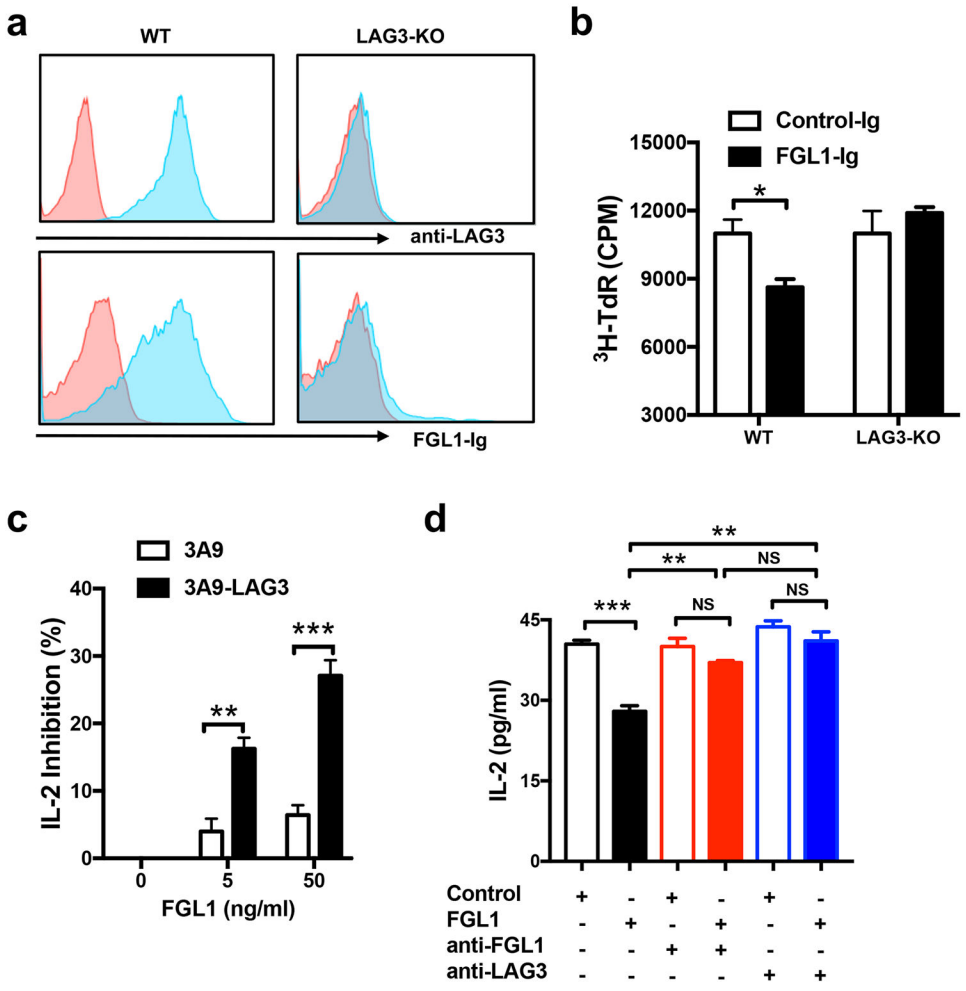

Figure 2. FGL1 mediates LAG3-dependent T cell suppression

(a) Splenic T cells from WT or LAG3-KO mice were activated by immobilized anti-CD3 mAb for 24 hours, stained with anti-LAG3 mAb or FGL1-Ig fusion protein (blue) or control antibody/Ig (red), and analyzed by flow cytometry.

(b) Splenic T cells from WT or LAG3-KO mice were activated by immobilized anti-CD3 mAb at suboptimal concentration in the presence of soluble FGL1-Ig or control-Ig (5ug/ml) for 3 days before the addition of ^{3}H-dTR. Thymidine incorporation of proliferated T cells was analyzed 16 hours later.

(c) The 3A9-LAG3 or parental 3A9 mouse T cell hybridoma cells were co-cultured with LK35.2 B cell line in CellGro serum free medium in the presence of HEL peptide and the indicated concentrations of FLAG-tagged FGL1. Shown is the normalized % of inhibition on the IL-2 levels in the supernatant at 24 hours normalized to levels with 0 ng/ml FGL1.

(d) The 3A9-LAG3 mouse T cell hybridoma cells were co-cultured with LK35.2 B cell line in the presence of HEL peptide, FLAG tagged FGL1 (50ng/ml), anti-FGL1, or anti-LAG3 mAb (1ug/ml). Shown are the IL-2 levels in the supernatant at 24 hours.

Data are representative of at least two independent experiments and are presented as the mean ± SEM. *$p < 0.05$, ** $p < 0.01$; *** $p<0.001$, NS, not significant by Student's t-test.

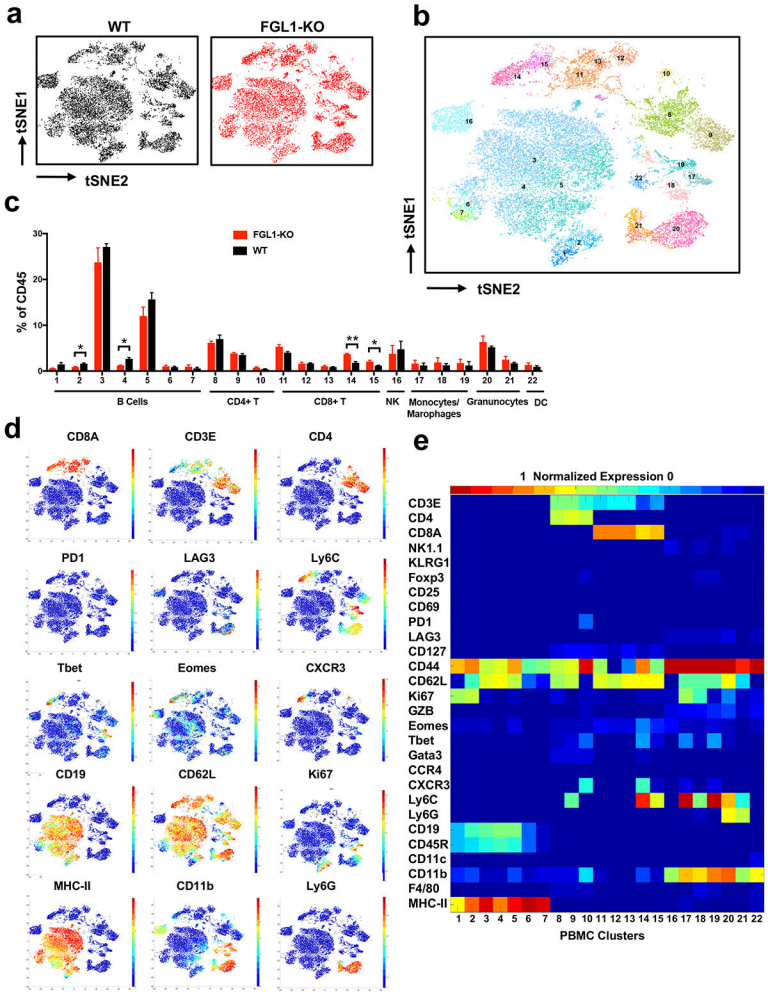

Figure 3. Immune cell phenotyping of FGL1-KO mice

(a) Density t-SNE plots of an equal number of CD45+ compartment in the peripheral blood from WT and FGL1-KO mice (n=3).

(b) t-SNE plot of CD45+ compartment overlaid with color-coded clusters.

(c) Frequency of clusters grouped by indicated immune cell subsets. Data were shown as the mean ± SEM. *, $p<0.05$; ** $p<0.01$ by unpaired t-test.

(d) t-SNE plot of CD45+ compartment overlaid with the expression of selected markers.

(e) Heatmap displaying normalized marker expression of each immune cluster.

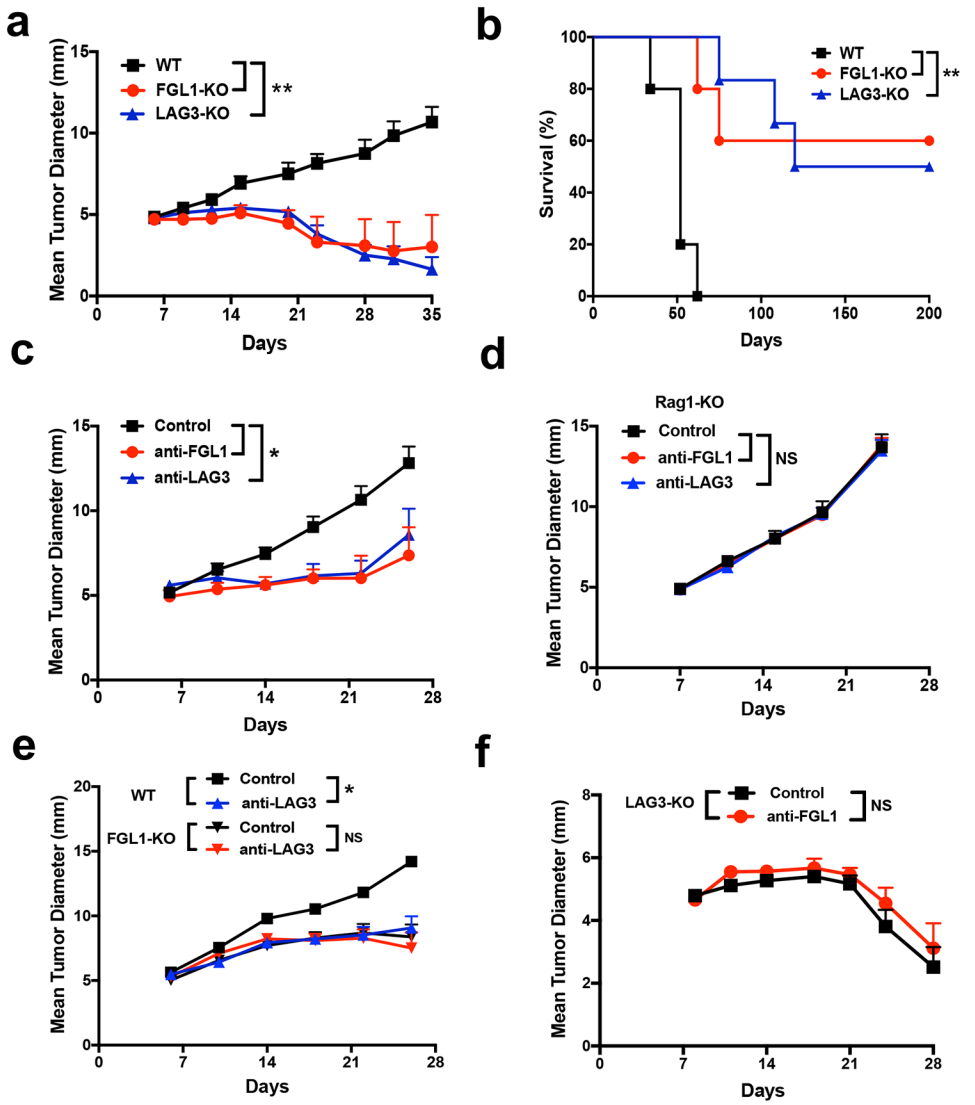

Figure 4. Ablation of the FGL1/LAG3 interaction inhibits tumor growth in mouse models

(a-b) FGL1-KO, LAG3-KO, or WT littermates were inoculated with MC38 cells (0.5×10^6/mouse). The mean tumor diameters (a) and survival (b) of mice in each group (n=6) are shown.

(c-d) B6 (c) or Rag1-KO (d) mice were inoculated with MC38 cells (0.5×10^6/mouse) at day 0 and treated with anti-FGL1, anti-LAG3, or control mAbs every four days from day 6 to day 18. The mean tumor diameters in each group (n=6) are shown.

(e) WT or FGL1-KO mice were inoculated with MC38 cells and were treated with anti-LAG3 or control mAb as in (c). The mean tumor diameters in each group (n=6–8) are shown.

(f) LAG3-KO mice were inoculated with MC38 cells and were treated with anti-FGL1 (n=8) or control mAb (n=7) as in (c). The mean tumor diameters in each group are shown.

Data were representative of at least two independent experiments and are shown as the mean ± SEM. *, $p<0.05$; **, $p<0.01$; NS, not significant. a, c-f by two-way ANOVA; b by Log-rank test.

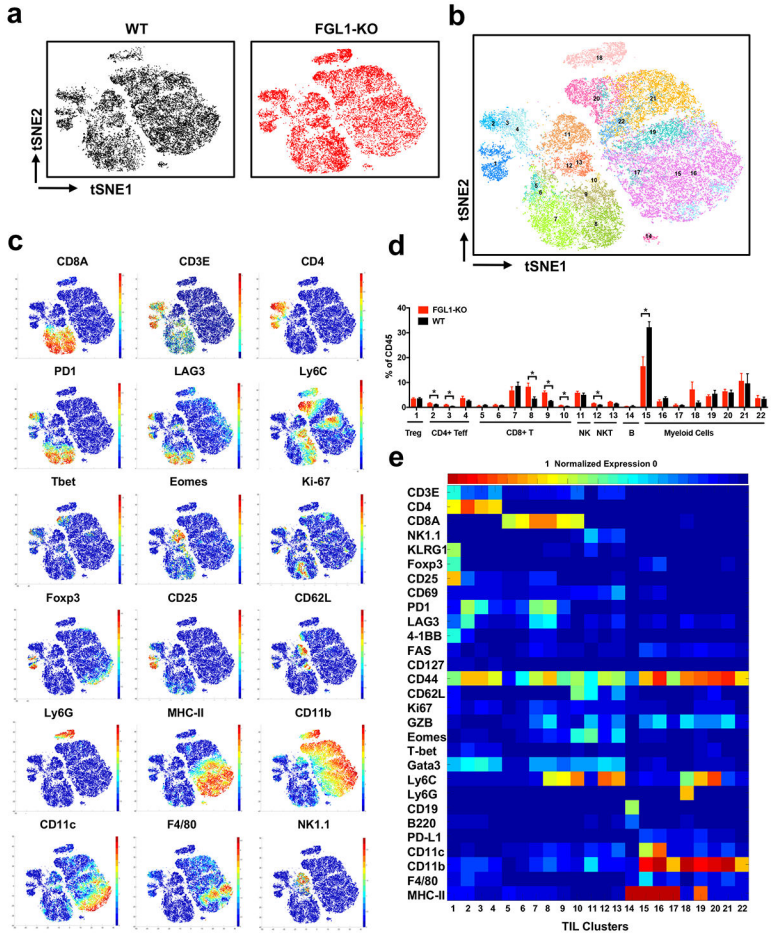

Figure 5. Expansion of tumor infiltrating T cell populations in FGL1-KO mice

(a) Density t-SNE plots of an equal number of CD45+ MC38 tumor-infiltrating leukocytes in WT (n=4) and FGL1-KO (n=5) mice. Size of unsupervised clusters denotes the relative number of cells in that grouping.

(b) t-SNE plot of tumor infiltrating leukocytes overlaid with color-coded clusters.

(c) t-SNE plot of tumor infiltrating leukocytes overlaid with the expression of selected markers.

(d) Frequency of clusters grouped by indicated immune cell subsets. Data were shown as the mean ± SEM. *, $p<0.05$ by unpaired t-test.

(e) Heatmap displaying normalized marker expression of each immune cluster.

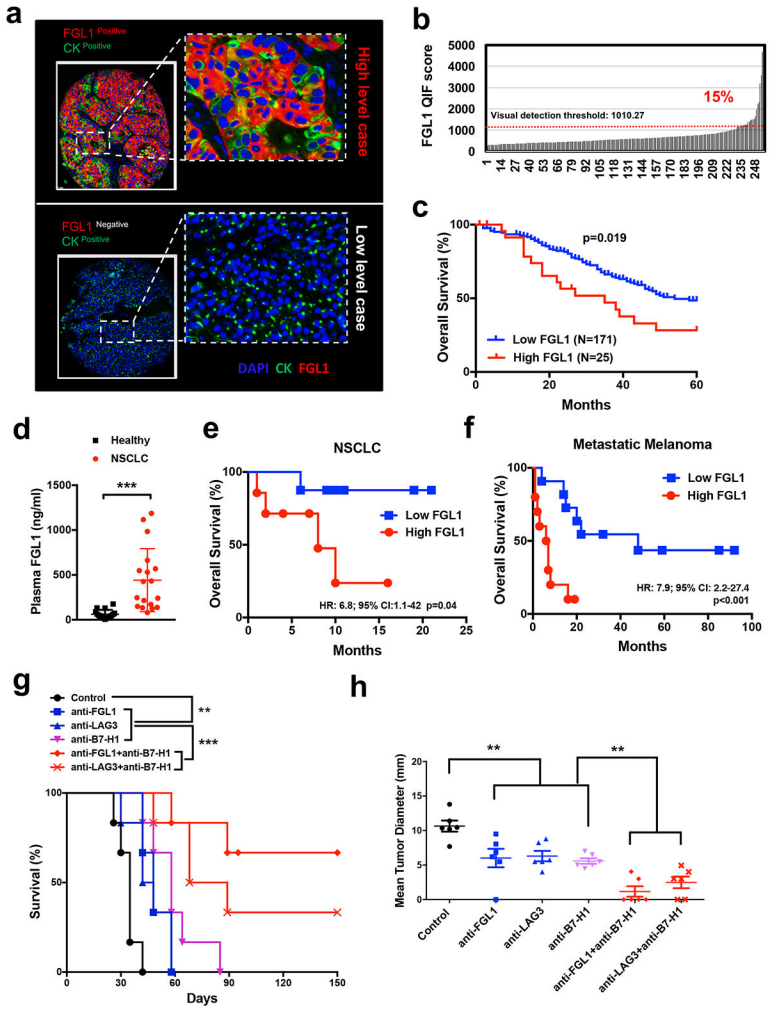

Figure 6. Upregulated FGL1 in human cancers is associated with a poor prognosis

(a) Representative immunofluorescence staining of FGL1, DAPI (for nuclear counterstain), and pancytokeratin (CK) in FGL1 positive or negative NSCLC cancer sections.

(b-c) FGL1 expression as indicated by quantitative immunofluorescence (QIF) staining in NSCLC cancer tissues from cohort #1 (see also Table S3). (b) Distribution of FGL1 expression, (c) association of high or low FGL1 expression with overall survival of the patients. The QIF visual detection threshold (1010.27) was used as a cutoff as indicated by dotted line in (b).

(d) The baseline plasma FGL1 levels were determined by ELISA in cohort #2 (see also Table S3) of NSCLC cancer patients (n=18) and healthy donors (n=16). Data were presented as the mean ± SEM. ***, $p<0.001$ by Student's t-test.

(e-f) Kaplan-Meier plots of overall survival stratified by median baseline plasma FGL1 levels in NSCLC (cut-point: 336.5 ng/ml) and melanoma (cut-point: 114 ng/ml) patients treated with single-agent antiPD-1 therapy in NSCLC (d, cohort #2, n=18) and melanoma (e, cohort #4, n=21), see also Table S3 and S4.

(g-h) B6 mice were inoculated *s.c.* with MC38 cells (0.5×10^6/mouse) at day 0, followed by the treatment with anti-FGL1, anti-LAG3, or control mAb (n=6 per group) every four days

from day 6 to day 18. In some groups, mice were also treated with a single dose of anti-B7-H1 (10B5) at day 6. (g) Survival of the mice is shown. Survival analysis was conducted by Log-rank test, **, $p<0.01$; ***, $p<0.001$. The presented data is representative of at least two independent experiments. (h) Tumor sizes are shown as the mean tumor diameter ± SEM at day 22. **, $p<0.01$ by Student's t-test.

KEY RESOURCES TABLE

REAGENT or RESOURCE	SOURCE	IDENTIFIER
Antibodies		
Anti-Mouse CD145 (clone 30-F11), 141-Pr	Fluidigm	Cat#: 3089005B
Anti-Mouse CD11c (clone N418), 142-Nd	Fluidigm	Cat#: 3142003B
Anti-Mouse CD69 (clone H1.2F3), 143-Nd	Fluidigm	Cat#: 3143004B
Anti-Mouse CD45R (clone RA3–6B2), 144-Nd	Fluidigm	Cat#: 3144011B
Anti-Mouse CD4 (clone RM4–5), 145-Nd	Fluidigm	Cat#: 3145002B
Anti-Mouse F4/80 (clone BM8), 146-Nd	Fluidigm	Cat#: 3146008B
Anti-Mouse FAS (clone SA367H8), 148-Nd	Biolegend	Cat#: 152602; RRID: AB_2629777
Anti-Mouse CD19 (clone 6D5), 149-Sm	Fluidigm	Cat#: 3149002B
Anti-Mouse CD25 (clone PC61), 150-Nd	Biolegend	Cat#: 102002; RRID: AB_312851
Anti-Mouse Ly6-G (clone 1A8), 151-Eu	Fluidigm	Cat#: 3151010B
Anti-Mouse CD3e (clone 145–2C11), 152-Sm	Fluidigm	Cat#: 3152004B
Anti-Mouse CD8a (clone 53–6.7), 153-Eu	Fluidigm	Cat#: 3153012B
Anti-Mouse KLRG-1 (clone 2F1), 154-Sm	Thermo Fisher	Cat#: 16–5893–82; RRID: AB_469131
Anti-Mouse CD28 (clone 37.51), 155-Gd	Thermo Fisher	Cat#: 16–0281–81; RRID: AB_468920
Anti-Mouse B7-H1 (clone 10B5), 156-Gd	*In-house*	
Anti-Mouse Foxp3 (clone FJK-16s), 158-Gd	Fluidigm	Cat#: 3158003A
Anti-Mouse PD-1 (clone 29F.1A12), 159-Tb	Fluidigm	Cat#: 3159024B
Anti-Mouse TBET (clone 4B10), 160-Gd	Fluidigm	Cat#: 3160010B
Anti-Mouse Ly6C (clone HK1.4), 162-Dy	Fluidigm	Cat#: 3162014B
Anti-Mouse CD62L (clone MEL-14), 164-Nd	Fluidigm	Cat#: 3164003B
Anti-Mouse 4–1BB (clone 2A), 166-Er	*In-house*	
Anti-Mouse KI-67 (clone B56), 168-Er	Fluidigm	Cat#: 3168007B
Anti-Mouse TIM-3 (clone RMT3–23), 169-Tm	Biolegend	Cat#: 119702; RRID: AB_345376
Anti-Mouse NK1.1 (clone PK136), 170-Er	Fluidigm	Cat#: 3170002B
Anti-Mouse CD44 (clone IM7), 171-Yb	Fluidigm	Cat#: 3171003B
Anti-Mouse CD11b (clone Ml/70), 172-Yb	Fluidigm	Cat#: 3172012B
Anti-Mouse Granzyme B (clone GB11), 173-Yb	Fluidigm	Cat#: 3173006B
Anti-Mouse LAG-3 (clone C9B7W), 174-Yb	Fluidigm	Cat#: 3174019B
Anti-Mouse CD127 (clone A7R34), 175-Lu	Fluidigm	Cat#: 3175006B
Anti-Mouse EOMES (clone Dan11mag), 176-Yb	Thermo Fisher	Cat#: 14–4875–80; RRID: AB_11043546
Anti-Mouse MHC class II (clone M5/114.15.2), 209-Bi	Fluidigm	Cat#: 3209006B
Anti-Mouse Pan-cytokeratin (CK, clone AE1/AE3)	Abcam	Cat#: ab27988
Anti-Mouse LAG-3 (clone 17B4)	Abcam	Cat#: ab40466
Anti-Mouse B7H1 (clone 405.9A11)	CST	Cat#: 29122
Anti-mouse CD3, functional grade	BD	Cat#: 553057
Secondary Anti-Mouse Envision	DAKO	Cat#: K4001

REAGENT or RESOURCE	SOURCE	IDENTIFIER
Secondary Goat Anti-Rabbit	Abeam	Cat#: ab6721
Secondary Anti-Mouse IgG1	Abeam	Cat#: ab97240
Anti-mouse FGL1 (clone 177R4)	This paper	N/A
Anti-mouse FGL1 (clone 177R1)	This paper	N/A
Anti-human FGL1 (clone 177 m03)	This paper	N/A
Anti-human FGL1 (clone 177 m01)	This paper	N/A
Anti-Mouse LAG3 (clone C9B7W), APC	Biolegend	Cat#: 125210
Anti-FLAG APC	Biolegend	Cat#: 637308
Alexa Fluor® 647 Goat Anti-Human IgG (H+L)	Invitrogen	Cat#: A-21445
Anti-mouse IgG APC	Biolegend	Cat#: 405308
TruStain fcX™ (anti-mouse CD16/32) Antibody	Biolegend	Cat#: 101320
Anti-mouse IgG HRP	Sigma	Cat#: A9044–2ML
Bacterial and Virus Strains		
Lenti-virus packaging kit	GeneCopoeia	Cat#: LT001
GeneCopoeia GCI-L3 chemically competent cells	GeneCopoeia	Cat#: STK-300–10
pLenti CMV Puro DEST (w118–1)	Addgene	Cat#: 17452
Biological Samples		
N/A		
Chemicals, Peptides, and Recombinant Proteins		
Collagenase from Clostridium Histolyticum, Type IV	Sigma-Aldrich	Cat#: C5138
DNase, Type I	Sigma-Aldrich	Cat#: D4527
Cell-ID Intercalator-Ir—125 μM	Fluidigm	Cat#: 201192A
Cell-ID Cisplatin	Fluidigm	Cat#: 201064
16% Paraformaldehyde Aqueous Solution, EM Grade	EMS	Cat#: 15710
TSA Plus Cy3 System	Perkin Elmer	Cat#: NEL744001KT
TSA Cy5-tyramide	Perkin Elmer	Cat#: SAT705A001EA
Biotinylated Tyramide	Perkin Elmer	Cat#: SAT700001EA
Streptavidin Alexa-750	Thermo Fisher	Cat # S-21384
DAPI (4’,6-Diamidino-2-Phenylindole, Dihydrochloride)	Thermo Fisher	Cat # D1306
I-Ak HEL peptide	MBL international	Cat# TS-M708-P
OVA 257–264 peptide	GenScript	Cat#: RP10611
Lipofectamine 2000	Invitrogen	Cat#:11668019
Critical Commercial Assays		
Mass cytometry antibody conjugation kits	Fluidigm	Cat#: 201300
Foxp3 / Transcription Factor Fixation/Permeabilization Concentrate and Diluent	Thermo Fisher	Cat#: 00–5521–00
EQTM Four Element Calibration Beads	Fluidigm	Cat#: 201078
Permeabilization Buffer (10X)	Thermo Fisher	Cat#: 00–8333–56

REAGENT or RESOURCE	SOURCE	IDENTIFIER
BD CBA mouse Inflammation/Th1,2,17 kit	BD Biosciences	Cat#:552364;560485
Mouse anti-dsDNA IgG specific ELISA kit	Alpha diagnostic International	Cat#: 5120
Octet Protein A Biosensor	PALL	https://www.fortebio.com/biosensors-Protein-A.html
Deposited Data		
CyTOF data for MC38 tumor from WT/FGL1-KO mice	This paper	Mendeley Data, see methods.
CyTOF data for PBMCs from WT/FGL1-KO mice	This paper	Mendeley Data, see methods.
Experimental Models: Cell Lines		
3A9	ATCC	Cat#: CRL3293
3A9-LAG3	Dr. Dario Vignali	Workman et al., 2002b
LK35.2	ATCC	Cat#: HB98
MC-38	NCI	Chen et al., 1994
Hepal-6	ATCC	Cat#: CRL1830
10B5(anti-B7-Hl/PD-Ll) Hybridoma	Chen Lab	Hirano et al., 2005
Recombinant DNA		
cDNA library	See methods	N/A
Software and Algorithms		
CyTOF Normalization	Finck et al., 2013	https://github.com/nolanlab/bead-normalization
X-Shift	Amusik et al., 2016	http://web.stanford.edu/$samusik/vortex/
Octet analysis software	PALL	https://www.fortebio.com/octet-software.html
R version 3.2	N/A	https://www.r-project.org/
FlowJo X 10.0.7r2	Flowjo, LLC	https://www.flowjo.com/
AQUA (automated quantitative analysis)	HistoRx	https://medicine.yale.edu/pathology/ypts/sts/servicemenu/qifaqua.aspx